Supplementary Information *for*

Land use interacts with changes in catchment hydrology to generate chronic nitrate pollution in karst waters and strong seasonality in excess nitrate export.

Fu-Jun Yue[1,2], Susan Waldron[1], Si-Liang Li[2*], Zhong-Jun Wang[3], Jie Zeng[3], Sen Xu[2], Zhi-Cai Zhang[4], David M. Oliver[5]

[1]School of Geographical and Earth Sciences, University of Glasgow, Glasgow G12 8QQ, United Kingdom;

[2]Institute of Surface-Earth System Science, Tianjin University, Tianjin 300072, China;

[3]State Key Laboratory of Environmental Geochemistry, Institute of Geochemistry, Chinese Academy of Sciences, Guiyang 550081, China;

[4]State Key Laboratory of Hydrology—Water Resources and Hydraulic Engineering, Hohai University, Nanjing 210098, China;

[5]Biological & Environmental Sciences, Faculty of Natural Sciences, University of Stirling, Stirling FK9 4LA, United Kingdom;

*Si-Liang Li (siliang.li@tju.edu.cn)

Contents：

technology measurements over a range of catchment scales.

3. Supplementary Figures

Figure S1: The linear relationship between sensor [NO_3^-–N] and laboratory [NO_3^-–N] measurement at Chenqi underground stream.

Figure S2: Time series of nitrate concentration and loading at five monitoring sites. The shaded cyan area associated with nitrate concentrations and loading represents the uncertainty in calculation.

Figure S3: Relationship between [NO_3^-–N] and discharge at Houzhai Catchment.

Figure S4: The relationship between the percentage of agricultural area and normalized NO_3^-–N export.

1. Supplementary Texts

Text S1: Sensor installation and calibration.

We used Hach nitrate ion-selective electrodes (NISE) sensors, which measure and compensate for chloride present in the water, thereby eliminating cross sensitivity between nitrate and chloride. The sensors with SC200 controllers were installed at the observatory stations and maintained at a fixed depth that ensured at least 30 cm of water above the sensor at all sites. The sensor collected data every 15 min with a response time of less than 3 min. Discrete stream water samples were collected manually at weekly or biweekly intervals, with additional samples collected during precipitation event periods using autosampler at intervals of one to four hours. Discrete samples for validation were collected, and immediately filtered for analysis. Samples for NO_3^- concentration were shipped to the laboratory after the field work and measured using an automatic flow analyzer (SKALAR Sans Plus Systems) with a detection limit of [NO_3^-–N] 10 μg/L.

The mv output may be affected by sensor fouling and cleaning. Therefore, if the fouling did not significantly impact on the measurement, the relationship between sensor [NO_3^-–N] and lab measured [NO_3^-–N] should be reasonably constant over time. We used linear relationship calibration between sensor [NO_3^-–N] and lab measured [NO_3^-–N] from discrete samples. To evaluate the second calibration processes, the uncertainty (μ_C) of time interval calibration and one single calibration at each site was compared (Table S2) This approach considered uncertainty in the laboratory measurements was negligible and the primary source of uncertainty was from the sensor measurement. The result showed lower uncertainty in the time interval calibration than in one single calibration. Figure S1 shows the time interval calibration process at Chenqi (CHQ) site. Finally, the time interval calibrated data were used as the final

[NO_3^-–N] at each site. The time series of [NO_3^-–N] and loading are shown in Figure S2 at all sites.

Text S2: Loading calculated method

Annual NO_3^-–N loading and normalized annual NO_3^-–N loading at each site were calculated following equations 1 and 2, respectively.

$$\text{Annual } NO_3^-\text{–N loading} = k \times \sum_{i=1}^{N} \frac{(C_i \times Q_i \times 60 \times 15)}{1000} \tag{1}$$

$$\text{Normalized Annual } NO_3^-\text{–N loading} = \frac{\text{Annual } NO_3^-\text{–N loading}}{A} \tag{2}$$

$$\left(\frac{\mu_L}{L}\right) = \sqrt{\left(\frac{\mu_C}{C}\right)^2 + \left(\frac{\mu_Q}{Q}\right)^2} \tag{3}$$

where C_i and Q_i are [NO_3^-–N] (mg/L) and discharge (m^3/s) with time interval 15mins. Constant k is 10^{-6} to convert units from mg/yr to kg/yr. N is the total number of measurements between November 2016 and October 2017 with time interval 15mins and A is catchment area and agricultural area in ha. The corresponding uncertainty of NO_3^-–N loading (μ_L) was estimated from sensor and discharge calibration by equation (3).

NO_3^-–N loading was calculated for missing time periods using linear interpolation for gaps less than 24h, whereas smoothed data using time-adjacent sensor measurements was applied for gaps exceeding 24h[1]. The proportion of missing and smoothed data in total annual data is less than 10% (Table S3), except at Houzhai River (HZ-R) owing to equipment damage by flow debris for the period 13th August - 6th October 2017. Grab sample data was also used to augment loading calculations for missing days of sensor data (which occurred due to temporary loss of power or minor issues with sensor performance). At HZ-R, [NO_3^-–N] loading was estimated using daily-collected samples during the period without sensor.

2. Supplementary Tables

Table S1: Summary of catchment characteristics basing on 2016 land use

	CHQ	CC	LHT	Houzhai (MSK &HZ-R)
Catchment area (km^2)	1.25	3.19	17.69	73.39
Natural vegetation (forest, shrub & grass, %)	82.8	66.6	59.2	45.1
Water area (river & reservoir, %)	0.0	0.1	0.4	1.4
Developed area (road & build area, %)	0.3	6.4	6.9	11.1
Farmland (dry land & paddy field, %)	16.7	26.0	32.7	41.0
Bare Rock (%)	0.3	0.8	0.7	1.4

Table S2: The uncertainty of two sensor calibration for each site at five sites during study period.

	Time interval calibration	One single calibration
	mg/L	mg/L
CHQ	0.06 – 0.64	1.02 – 1.41
CC	0.26 – 0.37	0.32 – 0.35
LHT	0.25 – 0.37	1.01 – 1.11
MSK	0.04 – 0.52	0.82 – 0.91
HZ–R	0.02 – 0.34	0.59 – 0.64

Table S3: Loading calculation for missing time periods.

	Missing data	Smoothed data
CHQ	7.8%	4.9%
CC	6.7%	0.3%
LHT	4.2%	1.6%
MSK	2.5%	0%
HZ-R	22.7%	17.3%

Table S4: Nine major intensive rain events during wet season in 2017.

	No.1	No.2	No.3	No.4	No.5	No.6	No.7	No.8	No.9
Date	5^{th} - 6^{th}	22th	3^{rd} - 5^{th}	12^{th}	15^{th}	24^{th}	29^{th} - 30^{th}	8^{th} - 9^{th}	1^{st} - 3^{rd}
	May		June					July	August
RF (mm)	41.4	69.2	31.2	101.5	34.6	65.1	85.9	127.4	49

Table S5 Comparison of annual normalised export generated from nitrate sensor technology measurements over a range of catchment scales.

	Country & studied year	Agricultural Land use (%)	Catchment size (ha)	Normalised export (kg/ha)
Houzhai (this study)	China (2016 – 2017)	41	7.34×10^{3}	22.2
Blackwater sub-catchment[2]	UK (2011 – 2012)	74	1.97×10^{3}	11.2 ± 3.9
Boone River at Webster[a3-4]	USA (2016)	84	2.19×10^{5}	72.3
Cedar River at Palo[a3-4]	USA (2016)	75	1.64×10^{6}	53.3
Iowa River at Wapello[a3-4]	USA (2016)	70	3.23×10^{6}	31.8
North Raccoon River[b3-4]	USA (2016)	80	4.2×10^{5}	50.4
Difficult Run[5]	USA (2016)	3	1.5×10^{4}	4.3
Smith Creek[5]	USA (2016)	46	2.5×10^{4}	6.0
Potomac River[5]	USA (2016)	30	3.0×10^{6}	5.3
Chemosit River[1]	Kenya (2014 – 2015)	52	1.0×10^{5}	4.6

[a] means catchments have more than 50% karst area; [b] means catchment have extensively artificial drainage consisting of underground networks and ditches.

3. Supplementary Figures

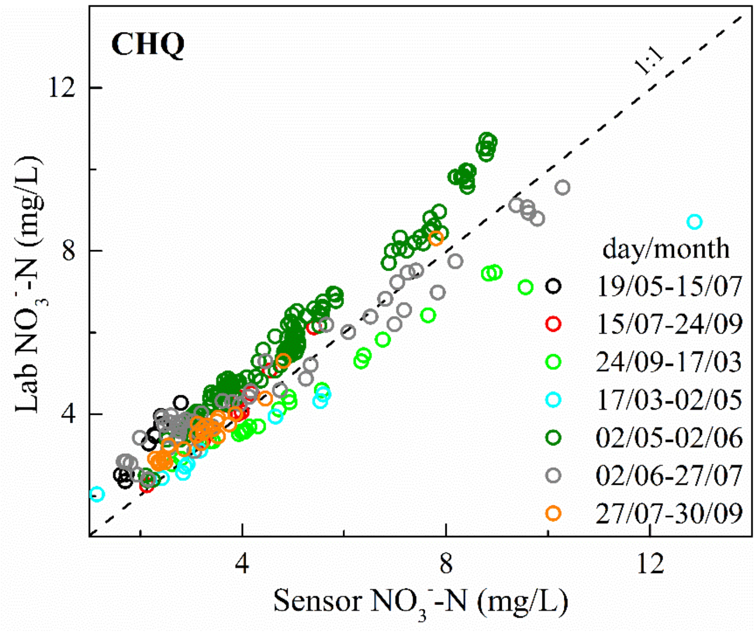

Figure S1: The linear relationship between sensor [NO_3^-–N] and laboratory [NO_3^-–N] measurement at Chenqi underground stream.

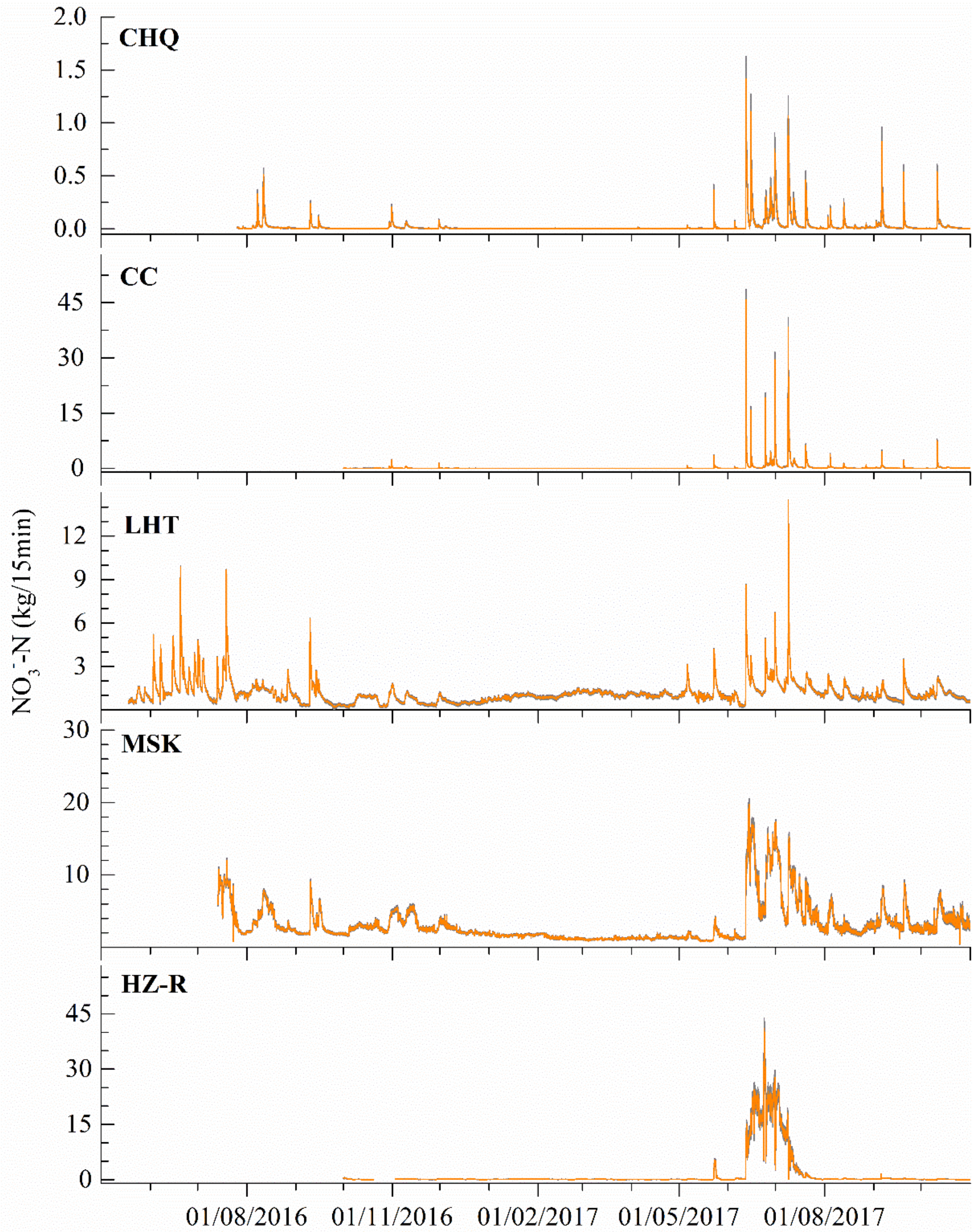

Figure S2: Time series of nitrate concentration and loading at five monitoring sites. The shaded cyan area associated with nitrate concentrations and loading represents the uncertainty in calculation.

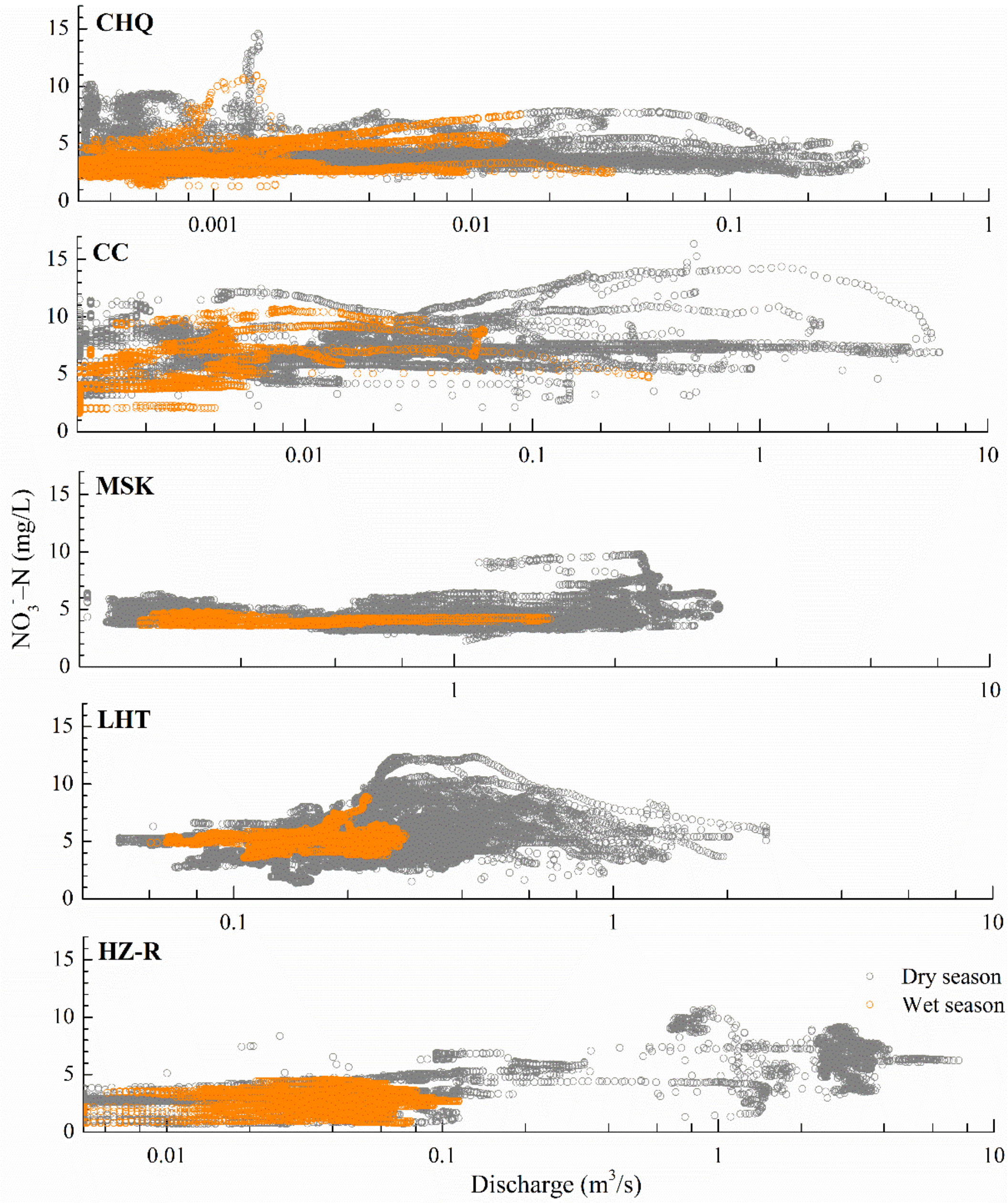

Figure S3: Relationship between [NO_3^-–N] and discharge at Houzhai Catchment.

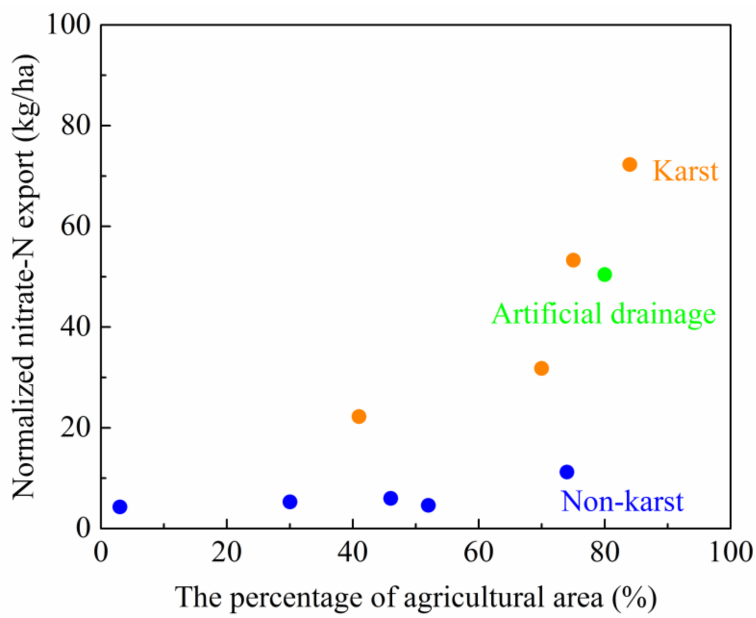

Figure S4: The relationship between the percentage of agricultural area and normalized nitrate-N export

Supplementary References:

(1) Jacobs, S. R.; Weeser, B.; Guzha, A. C.; Rufino, M. C.; Butterbach-Bahl, K.; Windhorst, D.; Breuer, L. (2018) Using high-resolution data to assess land use impact on nitrate dynamics in East African tropical montane catchments. Water Resour. Res. 54 (3), 1812-1830.

(2) Outram, F. N.; Cooper, R. J.; Sunnenberg, G.; Hiscock, K. M.; Lovett, A. A. (2016) Antecedent conditions, hydrological connectivity and anthropogenic inputs: Factors affecting nitrate and phosphorus transfers to agricultural headwater streams. Sci. Total Environ. 545, 184-199.

(3) Hansen, A.; Singh, A. (2018) High frequency sensor data reveal across-scale nitrate dynamics in response to hydrology and biogeochemistry in intensively managed agricultural basins. J. Geophys. Res-Biogeo. 123, 2168-2182.

(4) Jones, C. S.; Davis, C. A.; Drake, C. W.; Schilling, K. E.; Debionne, S. H. P.; Gilles, D. W.; Demir, I.; Weber, L. J. (2018) Iowa statewide stream nitrate load calculated using in situ sensor network. J. Am. Water Resour. As. 54 (2), 471-486.

(5) Miller, M. P.; Tesoriero, A. J.; Capel, P. D.; Pellerin, B. A.; Hyer, K. E.; Burns, D. A. (2016) Quantifying watershed-scale groundwater loading and in-stream fate of nitrate using high-frequency water quality data. Water Resour. Res. 52 (1), 330-347.